

Measurement of CP asymmetries in neutralino production at the ILC

O. Kittel^{a,1}, G. Moortgat-Pick^{b,c,2}, K. Rolbiecki^{c,3}, P. Schade^{c,d,4},
M. Terwort^{c,5}

^a *Departamento de Física Teórica y del Cosmos and CAFPE,
Universidad de Granada, E-18071 Granada, Spain*

^b *University of Hamburg, Luruper Chaussee 149, D-22761 Hamburg, Germany*

^c *DESY, Notkestrasse 85, D-22607 Hamburg, Germany*

^d *CERN, CH-1211 Geneve 23, Switzerland*

Abstract

We study the prospects to measure the CP-sensitive triple-product asymmetries in neutralino production $e^+ e^- \rightarrow \tilde{\chi}_i^0 \tilde{\chi}_1^0$ and subsequent leptonic two-body decays $\tilde{\chi}_i^0 \rightarrow \tilde{\ell}_R \ell$, $\tilde{\ell}_R \rightarrow \tilde{\chi}_1^0 \ell$, for $\ell = e, \mu$, within the Minimal Supersymmetric Standard Model. We include a full detector simulation of the International Large Detector for the International Linear Collider. The simulation was performed at a center-of-mass energy of $\sqrt{s} = 500$ GeV, including the relevant Standard Model background processes, a realistic beam energy spectrum, beam backgrounds and a beam polarization of 80% and -60% for the electron and positron beams, respectively. In order to effectively disentangle different signal samples and reduce SM and SUSY backgrounds we apply a method of kinematic reconstruction. Assuming an integrated luminosity of 500 fb^{-1} collected by the experiment and the performance of the current ILD detector, we arrive at a relative measurement accuracy of 10% for the CP-sensitive asymmetry in our scenario. We demonstrate that our method of signal selection using kinematic reconstruction can be applied to a broad class of scenarios and it allows disentangling processes with similar kinematic properties.

¹ kittel@th.physik.uni-bonn.de

² gudrid.moortgat-pick@desy.de

³ krzysztof.rolbiecki@desy.de

⁴ former address, schade.peter@web.de

⁵ mark.terwort@desy.de

1 Introduction

Supersymmetry (SUSY) [1, 2] is one of the best motivated candidates for physics beyond the Standard Model (SM). Besides providing a unification of the strong and electroweak gauge couplings and a suitable cold dark matter candidate, the lightest stable SUSY particle, SUSY could offer new sources of CP violation [3–6]. In the Minimal Supersymmetric Standard Model (MSSM), the complex parameters are conventionally chosen to be the Higgsino mass parameter μ , the U(1) and SU(3) gaugino mass parameters M_1 and M_3 , respectively, and the trilinear scalar coupling parameters A_f of the third generation sfermions ($f = b, t, \tau$),

$$\mu = |\mu|e^{i\phi_\mu}, \quad M_1 = |M_1|e^{i\phi_1}, \quad M_3 = |M_3|e^{i\phi_3}, \quad A_f = |A_f|e^{i\phi_{A_f}}. \quad (1)$$

The sizes of these phases are constrained by experimental bounds from the electric dipole moments (EDMs). Such experimental limits generally restrict the CP phases to be small, in particular the phase ϕ_μ [7]. However, the extent to which the EDMs can constrain the SUSY phases depends strongly on the considered model and its parameters [7–13].

Due to cancellations among different contributions to the EDMs, large CP phases can give CP-violating signals at colliders, as shown for example in Ref. [13]. It is important to search for these signals, since the cancellations could be a consequence of an unknown underlying structure that correlates the phases. In addition, the existing EDM bounds could also be fulfilled by including lepton flavor violating couplings in the slepton sector [9].

Thus, direct measurements of SUSY CP-sensitive observables are necessary to determine or constrain the phases independently of EDM measurements. The phases can change SUSY particle masses, their cross sections, branching ratios [14–18], and longitudinal polarizations of final fermions [19]. Although such CP-even observables can be very sensitive to the CP phases, CP-odd (T-odd) observables have to be measured for a direct evidence of CP violation.

CP asymmetries in particle decay chains can be defined with triple products of final particle momenta [20, 21]. Due to spin correlations, such asymmetries show unique hints for CP phases already at tree level. Thus, triple product asymmetries have been proposed in many theoretical papers. For the Large Hadron Collider (LHC), triple product asymmetries have been studied for the decays of neutralinos [22–24], stops [13, 25–27], sbottoms [28, 29], and staus [30]. In a Monte Carlo (MC) analysis for stop decays [26, 27], it could be shown that the decay chain can be reconstructed and asymmetries be measured at a 3σ level for luminosities of the order of 300 fb^{-1} . At the International Linear Collider (ILC) [31–34] a clearer identification and a more precise measurement is expected to be achievable. However, in this context only theoretically-based papers exist: for instance, neutralino production with two- [22, 35–42] and three-body decays [43–47], charginos with two- [48–53] and three-body decays [54, 55], also with transversely polarized beams [56–61], have been studied.

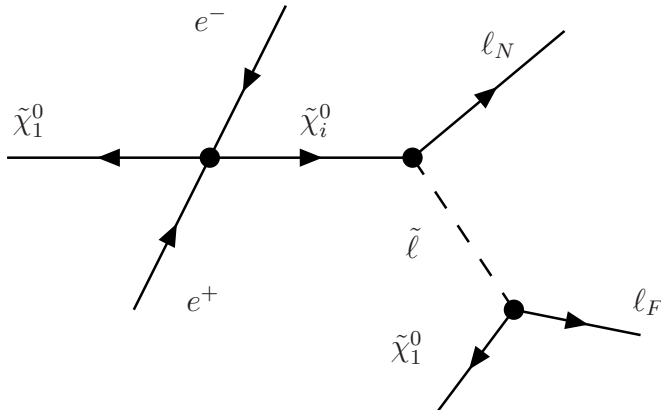


Figure 1: Schematic picture of neutralino production and decay.

Therefore, we present in this paper the first experimentally-oriented analysis with regard to the observation of CP asymmetries on the basis of a full detector simulation. To show the feasibility of a measurement of triple product asymmetries, we focus on neutralino production [35, 39]

$$e^+ + e^- \rightarrow \tilde{\chi}_i^0 + \tilde{\chi}_1^0 \quad (2)$$

with longitudinally polarized beams and the subsequent leptonic two-body decay of one of the neutralinos into the near lepton

$$\tilde{\chi}_i^0 \rightarrow \tilde{\ell}_R + \ell_N, \quad (3)$$

and that of the slepton into a far lepton

$$\tilde{\ell}_R \rightarrow \tilde{\chi}_1^0 + \ell_F; \quad \ell = e, \mu. \quad (4)$$

Fig. 1 shows a schematic picture of neutralino production and its decay chain. The CP-sensitive spin correlations of the neutralino in its production process allow us to probe the phase of the Higgsino mass parameter μ , and the gaugino parameter M_1 .

In order to effectively disentangle different signal samples and reduce SM and SUSY backgrounds we apply a method of kinematic reconstruction. A similar approach has been studied successfully for the LHC [27]. The kinematic reconstruction was also considered to study selectron and neutralino properties at the ILC [62–64]. Here, we demonstrate that it can be used as an effective signal selection method, greatly improving the sensitivity to the effects of CP violation. In particular, compared to the previous studies of process (2), Ref. [39], we are able to suppress slepton and WW contamination to $\mathcal{O}(10\%)$ level.

To investigate in detail the prospect of measuring CP-sensitive observables at the ILC we perform a full detector simulation of the International Large Detector (ILD) concept. We include all relevant SM and SUSY background processes in our study, simulated with a realistic beam energy spectrum (beamstrahlung and initial state radiation (ISR)), beam backgrounds and a beam polarization of

$(P_{e^-}, P_{e^+}) = (0.8, -0.6)$, which enhances the cross section of our signal and the size of the asymmetry. We apply the method of kinematic reconstruction to a preselected sample of signal event candidates in order to efficiently reject any background and to disentangle the decays of $\tilde{\chi}_2^0$ from $\tilde{\chi}_3^0$. We determine the CP asymmetries with the selected signal events and study the sensitivity to determine the values of the CP phases via a fit.

The paper is organized as follows. In Sec. 2 we introduce the theoretical framework for the used CP-sensitive observable and we apply it for the studied process in the chosen benchmark scenario. Section 3 discusses the kinematic aspects of signal versus background selection. Section 4 treats the full detector simulation. Finally in Sec. 5 the SUSY parameters including the CP phases are derived via a fit of the CP-odd asymmetries together with masses and cross sections. Appendix A provides details for the reconstruction of W and $\tilde{\ell}$ production and App. B recapitulates the neutralino mixing and its parameters.

2 Theoretical framework

2.1 CP-odd observables

CP-violating observables in collider-based experiments are based on the invariance under CPT_N , where C is charge conjugation, P stands for parity transformation and T for time reversal. The index N denotes 'naive' time reversal, i.e. time reversal but without interchanging initial with final states and therefore can be tested in collider-based experiments. At tree level of perturbation theory, observables odd under T_N transformations are also odd under the 'true' time reversal T.

Therefore, it is useful to categorize CP-violating observables in two classes [65]: those that are even under T_N and those that are odd under T_N operation. Under the absence of final state interactions (FSI), CPT_N -even operators relate T_N -odd symmetries uniquely with CP-odd transformations [20]. Contrary, CPT_N -odd operators (i.e. CP-odd but T_N -even) can have nonzero expectation values only if FSI are present that give a non-trivial phase (absorptive phase) to the amplitude. Such a phase can arise for instance in loop diagrams.

Examples for T_N -odd observables are triple products that arise from the terms $\epsilon[p_1, p_2, p_3, p_4]$, where p_i are 4-vectors representing spins or momenta and ϵ is the antisymmetric Levi-Civita tensor. Consequently, such T_N -odd signals can only be observed in processes where at least four independent momenta (or their spin orientations) are involved. The ϵ -tensor can then be expanded in a series of four triple products $\epsilon[p_1, p_2, p_3, p_4] = E_1 \mathbf{p}_2 \cdot (\mathbf{p}_3 \times \mathbf{p}_4) \pm \dots$ that can be evaluated in a suitable and specific kinematical system. The T_N -odd asymmetries are then composed by the corresponding triple products.

2.2 Neutralino production and decay processes

Neutralinos are mixed states of the supersymmetric partners of the neutral gauge and Higgs bosons and depend on the phases ϕ_1 and ϕ_μ , see App. B. CP-violating

effects in the neutralino production and decay arise at tree level and can lead to CP-sensitive asymmetries due to neutralino spin correlations.

In neutralino production effects from CP-violating phases can only occur if two different neutralinos are produced, $e^+e^- \rightarrow \tilde{\chi}_i^0 \tilde{\chi}_j^0$, $i \neq j$. Each of the produced neutralinos has a polarization with a component normal to the production plane [44, 66, 67]. This polarization leads to asymmetries in the angular distributions of the decay products.

In our process the only T_N -odd contribution originates from the production process. It is proportional to $\epsilon[p_{e^+} p_{e^-} s_{\tilde{\chi}_i^0} p_{\tilde{\chi}_i^0}]$ leading to $\epsilon[p_{e^+} p_{e^-} p_{\ell_N} p_{\tilde{\ell}_R}]$ due to spin correlations caused by the mentioned neutralino polarization normal to the production plane. Applying momentum conservation $p_{\tilde{\ell}_R} = p_{\tilde{\chi}_1^0} + p_{\ell_F}$ allows one to extract the T_N -odd triple product of the beam and the final lepton momenta [35],

$$\mathcal{T} = (\mathbf{p}_{e^-} \times \mathbf{p}_{\ell_N^+}) \cdot \mathbf{p}_{\ell_F^-} \equiv (\mathbf{p}_{e^-}, \mathbf{p}_{\ell_N^+}, \mathbf{p}_{\ell_F^-}), \quad (5)$$

which projects out the CP-sensitive parts. The corresponding T_N -odd asymmetry is then

$$\mathcal{A}(\mathcal{T}) = \frac{\sigma(\mathcal{T} > 0) - \sigma(\mathcal{T} < 0)}{\sigma(\mathcal{T} > 0) + \sigma(\mathcal{T} < 0)}, \quad (6)$$

where σ is the cross section for neutralino production and decay, Eqs. (2)-(4). Note: in the case of the 3-body neutralino decay, $\tilde{\chi}_i^0 \rightarrow \ell^+ \ell^- \tilde{\chi}_1^0$, one also obtains T_N -odd contributions originating only from the decay process [26, 47]. Therefore further T_N -odd asymmetries can be composed that contribute also in case of same-neutralino pair production and can offer tools for disentangling the different phases. The CP-sensitive asymmetries, Eq. (6), depend on the charge of the leptons [13] and the following relations are given:

$$\begin{aligned} \mathcal{A}(\mathbf{p}_{e^-}, \mathbf{p}_{\ell_N^+}, \mathbf{p}_{\ell_F^-}) &= -\mathcal{A}(\mathbf{p}_{e^-}, \mathbf{p}_{\ell_N^-}, \mathbf{p}_{\ell_F^+}) \\ &= -\mathcal{A}(\mathbf{p}_{e^-}, \mathbf{p}_{\ell_F^-}, \mathbf{p}_{\ell_N^+}) \\ &= +\mathcal{A}(\mathbf{p}_{e^-}, \mathbf{p}_{\ell_F^+}, \mathbf{p}_{\ell_N^-}), \end{aligned} \quad (7)$$

neglecting FSI contributions. Note that a true CP-odd asymmetry, where also an absorptive phase from FSI or finite-width effects is automatically eliminated, can be defined as

$$\mathcal{A}^{\text{CP}} = \frac{1}{2}(\mathcal{A} - \bar{\mathcal{A}}), \quad (8)$$

where $\bar{\mathcal{A}}$ denotes the T_N -odd asymmetry for the CP-conjugated process [68]. In our case this leads to a separate measurement of asymmetries for a positive (ℓ_N^+) and negative (ℓ_N^-) near lepton. If $\mathcal{A}^{\text{CP}} \neq 0$ holds than we observe a genuine CP-violating effect. Therefore, it is important to tag the charge of the near and far leptons in order to establish CP violation in the process (2)-(4).

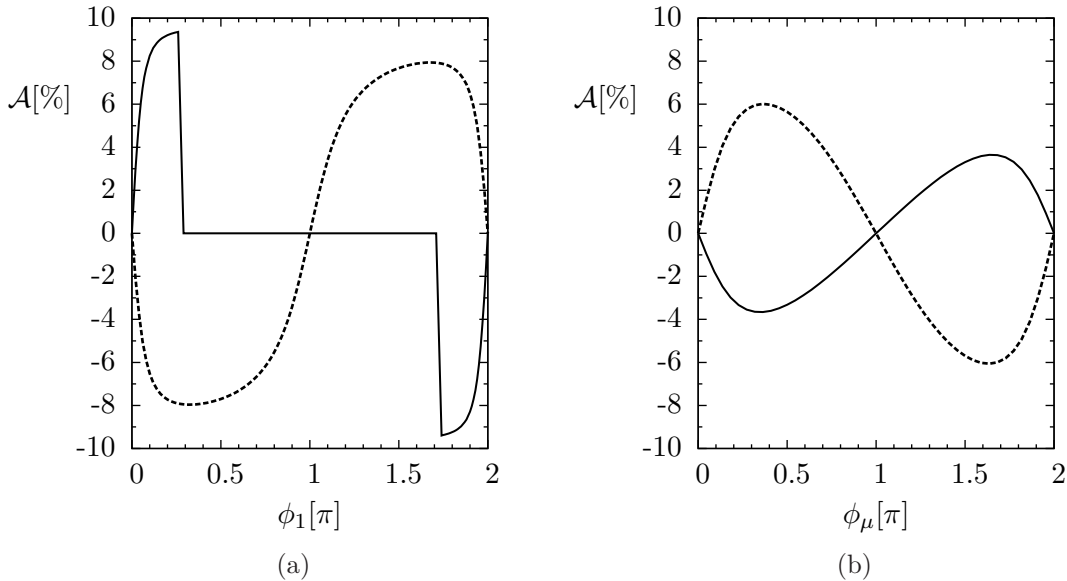


Figure 2: Dependence of the asymmetry \mathcal{A} , Eq. (6), (a) on the phase ϕ_1 (with $\phi_\mu = 0$), (b) the phase ϕ_μ (with $\phi_1 = 0$), for neutralino production $e^+e^- \rightarrow \tilde{\chi}_1^0 \tilde{\chi}_2^0$ (solid), and $e^+e^- \rightarrow \tilde{\chi}_1^0 \tilde{\chi}_3^0$ (dashed), and subsequent decay $\tilde{\chi}_i^0 \rightarrow \tilde{\ell}_R \ell_N$, $\tilde{\ell}_R \rightarrow \tilde{\chi}_1^0 \ell_F$, (for $\ell = e$ or μ), at $\sqrt{s} = 500$ GeV and polarized beams $(P_{e^-}, P_{e^+}) = (0.8, -0.6)$. The other MSSM parameters are given in Tab. 1. In the left panel, along the flat line of the asymmetry (solid) the decay $\tilde{\chi}_2^0 \rightarrow \tilde{\ell}_R \ell$ is closed.

M_2	$ M_1 $	$ \mu $	ϕ_1	ϕ_μ	$\tan \beta$	$M_{\tilde{E}}$	$M_{\tilde{I}}$
300 GeV	150 GeV	165 GeV	0.2π	0	10	166 GeV	280 GeV

Table 1: MSSM parameters of the benchmark scenario at the electroweak scale, see Sec. 2.3.

2.3 Benchmark scenario

For our full simulation study, we have chosen a benchmark scenario with the relevant MSSM parameters given in Tab. 1. Since the phase of the Higgsino mass parameter is strongly constrained by EDM bounds, we have set it to zero. The value of the gaugino phase $\phi_1 = 0.2\pi$ approximately corresponds to the maximum of the CP asymmetries, see Fig. 2. The scenario was chosen to have an enhanced neutralino mixing close to a level-crossing of the neutralino states $\tilde{\chi}_2^0$ and $\tilde{\chi}_3^0$ for $\phi_1 = 0$, and of $\tilde{\chi}_1^0$ and $\tilde{\chi}_2^0$ for $\phi_1 = \pi$, which leads to large CP asymmetries.

Further, we have assumed beam polarizations of $(P_{e^-}, P_{e^+}) = (0.8, -0.6)$ enhancing slightly the SUSY cross section and the asymmetries. At the same time, this choice suppresses the background from WW -pair production, $\sigma(e^+e^- \rightarrow WW) = 0.7$ pb (compared with 7 pb for unpolarized beams), and also chargino pair produc-

masses	$m_{\tilde{\chi}_1^0} = 117 \text{ GeV}$	$m_{\tilde{\ell}_R} = 166 \text{ GeV}$
	$m_{\tilde{\chi}_2^0} = 169 \text{ GeV}$	$m_{\tilde{\ell}_L} = 280 \text{ GeV}$
	$m_{\tilde{\chi}_3^0} = 181 \text{ GeV}$	$m_{\tilde{\tau}_1} = 165 \text{ GeV}$
	$m_{\tilde{\chi}_4^0} = 330 \text{ GeV}$	$m_{\tilde{\tau}_2} = 280 \text{ GeV}$
	$m_{\tilde{\chi}_1^\pm} = 146 \text{ GeV}$	$m_{\tilde{\nu}} = 268 \text{ GeV}$
	$m_{\tilde{\chi}_2^\pm} = 330 \text{ GeV}$	$m_{\tilde{\nu}_\tau} = 268 \text{ GeV}$
cross sections	$\sigma(e^+e^- \rightarrow \tilde{\chi}_1^0\tilde{\chi}_2^0) = 244 \text{ fb}$	$\sigma(e^+e^- \rightarrow \tilde{e}_R^+\tilde{e}_R^-) = 304 \text{ fb}$
	$\sigma(e^+e^- \rightarrow \tilde{\chi}_1^0\tilde{\chi}_3^0) = 243 \text{ fb}$	$\sigma(e^+e^- \rightarrow \tilde{\mu}_R^+\tilde{\mu}_R^-) = 97 \text{ fb}$
branching ratios	$\text{BR}(\tilde{\chi}_2^0 \rightarrow \tilde{\ell}_R\ell) = 55\%$	$\text{BR}(\tilde{\chi}_2^0 \rightarrow \tilde{\tau}_1\tau) = 45\%$
	$\text{BR}(\tilde{\chi}_3^0 \rightarrow \tilde{\ell}_R\ell) = 64\%$	$\text{BR}(\tilde{\chi}_3^0 \rightarrow \tilde{\tau}_1\tau) = 36\%$
asymmetries	$\mathcal{A}(\mathcal{T})_{\tilde{\chi}_1^0\tilde{\chi}_2^0} = -9.2\%$	$\mathcal{A}(\mathcal{T})_{\tilde{\chi}_1^0\tilde{\chi}_3^0} = 7.7\%$

Table 2: Masses, production cross sections, neutralino branching ratios and asymmetries, Eq. (6), for the benchmark scenario, see Tab. 1, calculated using the formulas presented in [42]. The ILC cross sections are for $\sqrt{s} = 500 \text{ GeV}$ and polarized beams $(P_{e^-}, P_{e^+}) = (0.8, -0.6)$. The branching ratios are summed over $\ell = e, \mu$ and both slepton charges.

tion $\sigma(e^+e^- \rightarrow \tilde{\chi}_i^\pm\tilde{\chi}_j^\mp) = 110 \text{ fb}$ (410 fb, respectively). Thus, the scenario is optimized to yield large asymmetries, large cross sections and sizable neutralino branching ratios into electrons and muons, as listed in Tab. 2. We have set $A_\tau = -250 \text{ GeV}$ in the stau sector, which has low impact on the neutralino branching ratios. Also we have chosen the slepton masses such that $\tilde{\chi}_2^0$ is close in mass with the slepton $\tilde{\ell}_R$. This leads to soft leptons from the decay $\tilde{\chi}_2^0 \rightarrow \tilde{\ell}_R\ell$, as can be seen in Fig. 3, which has to be taken care of in the lepton identification described in Sec. 4.2.

In general, our analysis is relevant for scenarios with strong gaugino-higgsino mixing in the neutralino sector, usually leading to sizable asymmetries. In particular, for $|\mu| \lesssim |M_2| \lesssim 300 \text{ GeV}$ the asymmetries can reach several percent, the neutralino pair-production cross sections reach more than 50 fb, and the neutralino branching ratios into electrons and muons are of the order of several 10%, see also Ref. [35] for more details. In any case, the selectron and smuon masses should fulfil $m_{\tilde{\chi}_1^0} < m_{\tilde{\ell}_R} < m_{\tilde{\chi}_2^0}$, so that at least one relevant decay channel remains open. Decreasing the selectron mass will result in larger asymmetries and production cross sections.

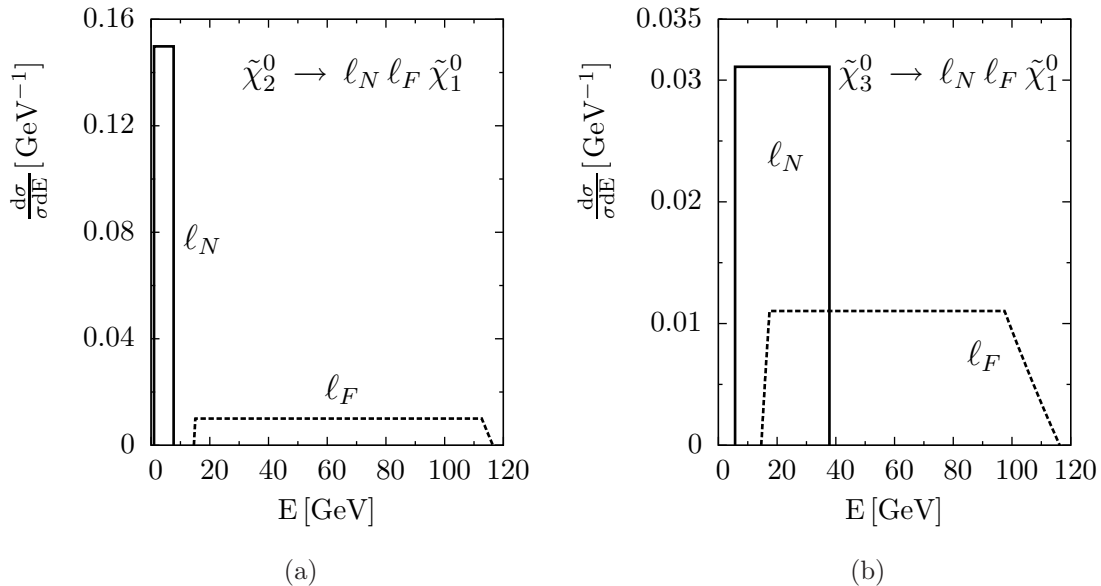


Figure 3: Energy distributions (each normalized to 1) of the near lepton ℓ_N (solid), and the far lepton ℓ_F (dashed), from neutralino production $e^+e^- \rightarrow \tilde{\chi}_1^0 \tilde{\chi}_i^0$ for (a) $i = 2$, and (b) $i = 3$, with subsequent decay $\tilde{\chi}_i^0 \rightarrow \tilde{\ell}_R \ell_N$, $\tilde{\ell}_R \rightarrow \tilde{\chi}_1^0 \ell_F$, for the benchmark scenario as given in Tabs. 1 and 2.

3 Kinematic selection of signal and background

In order to measure the CP asymmetries, Eq. (6), we have to separate the signal lepton pairs originating from $\tilde{\chi}_1^0 \tilde{\chi}_2^0$ and $\tilde{\chi}_1^0 \tilde{\chi}_3^0$ production, respectively. This is essential, since in our scenario the corresponding CP asymmetries, $\mathcal{A}(\tilde{\chi}_1^0 \tilde{\chi}_2^0) = -9.2\%$ and $\mathcal{A}(\tilde{\chi}_1^0 \tilde{\chi}_3^0) = 7.7\%$, have opposite sign. Large CP asymmetries naturally occur when the neutralinos are mixed states of gauginos and Higgsinos, which often implies that they are close in mass. In addition we need an efficient method for background separation. The CP-even backgrounds will reduce the asymmetries, since they contribute to the denominator, but cancel out in the numerator of the asymmetries, see Eq. (6). Among the most severe SM and SUSY background processes are W pair production and slepton pair production.

Owing to a known center-of-mass energy and a well-defined initial state one may attempt to perform a full kinematic reconstruction of the events at the ILC. Unlike in the case of the LHC [24,27], this is already possible with very short decay chains. Assuming that the masses of intermediate and invisible particles are known from other measurements, the full reconstruction can be performed even when only two particles are visible in the final state.

In the following, we extend the method of Ref. [58] to reconstruct the pair of signal leptons from the neutralino decay, Eq. (2). We show that even for two neutralino states that are close in mass, here $\tilde{\chi}_2^0$ and $\tilde{\chi}_3^0$, the final leptons can be correctly

assigned to their mother particle. A similar procedure to identify and suppress background from W and slepton pair production is described in App. A, see also Ref. [69]. Finally, we discuss how well the kinematic selection and reconstruction works at the MC level.

3.1 Kinematic constraints from neutralino production

In the center-of-mass system of neutralino pair production the momenta and energies are fixed [67] :

$$E_{\tilde{\chi}_i^0} = \frac{s + m_{\tilde{\chi}_i^0}^2 - m_{\tilde{\chi}_j^0}^2}{2\sqrt{s}}, \quad E_{\tilde{\chi}_j^0} = \frac{s + m_{\tilde{\chi}_j^0}^2 - m_{\tilde{\chi}_i^0}^2}{2\sqrt{s}}, \quad |\mathbf{p}_{\tilde{\chi}_{i,j}^0}| = \frac{\lambda^{\frac{1}{2}}(s, m_{\tilde{\chi}_i^0}^2, m_{\tilde{\chi}_j^0}^2)}{2\sqrt{s}}, \quad (9)$$

with the beam energy $E = \sqrt{s}/2$, the neutralino masses $m_{\tilde{\chi}_i^0}, m_{\tilde{\chi}_j^0}$, and $\lambda(x, y, z) = x^2 + y^2 + z^2 - 2(xy + xz + yz)$. The neutralino production is followed by the two-body decay chain of one of the neutralinos $\tilde{\chi}_i^0$ via a slepton,

$$\tilde{\chi}_i^0 \rightarrow \tilde{\ell}_R + \ell_N \rightarrow \tilde{\chi}_1^0 + \ell_F + \ell_N, \quad \ell = e, \mu. \quad (10)$$

In our signal process, Eqs. (2)-(4), we have $\tilde{\chi}_j^0 = \tilde{\chi}_1^0$ and it escapes undetected.

In the following, we assume that the near and far leptons can be distinguished via their different energy distributions.⁶ For our scenario, the leptons from $\tilde{\chi}_1^0\tilde{\chi}_2^0$ production and decay have distinct energy ranges, see Fig. 3(a). The leptons from $\tilde{\chi}_1^0\tilde{\chi}_3^0$ production and decay only have a small overlap in the energy window $E_\ell \in [18, 38]$ GeV, see Fig. 3(b). Events are discarded if both leptons happen to fall into this energy range. We now choose a coordinate system such that the measured momenta are

$$\mathbf{p}_{\ell_N} = |\mathbf{p}_{\ell_N}| (0, 0, 1), \quad (11)$$

$$\mathbf{p}_{\ell_F} = |\mathbf{p}_{\ell_F}| (\sin \theta_{NF}, 0, \cos \theta_{NF}), \quad \theta_{NF} \in [0, \pi], \quad (12)$$

where θ_{NF} is the angle between the near and the far leptons. In order to fully reconstruct the event, the decay angles of the sleptons need to be resolved

$$\mathbf{p}_{\tilde{\ell}} = |\mathbf{p}_{\tilde{\ell}}| (\sin b \cos B, \sin b \sin B, \cos b), \quad b \in [0, \pi], \quad B \in [0, 2\pi]. \quad (13)$$

The slepton momentum, $\mathbf{p}_{\tilde{\ell}}^2 = E_{\tilde{\ell}}^2 - m_{\tilde{\ell}}^2$, is already fixed due to energy conservation, $E_{\tilde{\ell}} = E_{\tilde{\chi}_i^0} - E_{\ell_N}$. Using also momentum conservation, $\mathbf{p}_{\tilde{\chi}_i^0}^2 = (\mathbf{p}_{\ell_N} + \mathbf{p}_{\tilde{\ell}})^2$, the polar angle, $b = \sphericalangle(\mathbf{p}_{\ell_N}, \mathbf{p}_{\tilde{\ell}})$, can be determined

$$\cos b = \frac{\mathbf{p}_{\tilde{\chi}_i^0}^2 - \mathbf{p}_{\ell_N}^2 - \mathbf{p}_{\tilde{\ell}}^2}{2|\mathbf{p}_{\ell_N}||\mathbf{p}_{\tilde{\ell}}|}, \quad \sin b = +\sqrt{1 - \cos^2 b}. \quad (14)$$

⁶This is not needed for the determination of the asymmetry, see Eq. (7), but will be exploited for the event selection.

Using also momentum conservation in the slepton decay, $\mathbf{p}_{\tilde{\ell}} = \mathbf{p}_{\ell_F} + \mathbf{p}_{\tilde{\chi}_1^0}$, a similar relation can be obtained for the azimuthal angle

$$\cos B = \frac{1}{\sin b \sin \theta_{NF}} \left(\frac{\mathbf{p}_{\ell_F}^2 + \mathbf{p}_{\tilde{\ell}}^2 - \mathbf{p}_{\tilde{\chi}_1^0}^2}{2|\mathbf{p}_{\ell_F}||\mathbf{p}_{\tilde{\ell}}|} - \cos b \cos \theta_{NF} \right), \quad (15)$$

and $\mathbf{p}_{\tilde{\chi}_1^0}^2 = E_{\tilde{\chi}_1^0}^2 - m_{\tilde{\chi}_1^0}^2$ is obtained from energy conservation $E_{\tilde{\chi}_1^0} = E_{\tilde{\chi}_i^0} - E_{\ell_N} - E_{\ell_F}$. The kinematic variables $\cos b$ and $\cos B$ solely depend on the center-of-mass energy s , the lepton energies, E_{ℓ_N} and E_{ℓ_F} , the angle between the leptons, $\mathbf{p}_{\ell_N} \cdot \mathbf{p}_{\ell_F}$, and finally on the contributing particle masses, $m_{\tilde{\chi}_i^0}$, $m_{\tilde{\chi}_1^0}$, and $m_{\tilde{\ell}_R}$. Thus, there only remains an ambiguity for $\sin B$, since for $B \in [0, 2\pi]$ we have $\sin B = \pm \sqrt{1 - \cos^2 B}$. This ambiguity in the azimuthal angle is irrelevant for the efficiency of the event selection⁷.

3.2 Method of kinematic event selection

For a given lepton pair, we apply the following kinematic selection method. The aim is to assign the correct origin of the lepton pair, which can be signal, $e^+e^- \rightarrow \tilde{\chi}_i^0 \tilde{\chi}_1^0$, or background $e^+e^- \rightarrow W^+W^-$, $\tilde{\ell}_R^+ \tilde{\ell}_R^-$. Thus, we have four systems of equations, one for each possible production process. For each candidate event we employ the following kinematic selection:

- We apply the reconstruction procedure from Sec. 3.1, assuming $\tilde{\chi}_1^0 \tilde{\chi}_2^0$ and $\tilde{\chi}_1^0 \tilde{\chi}_3^0$ production. Thus, we calculate $\cos b$ and $\cos B$, Eqs. (14) and (15), with $m_{\tilde{\chi}_i^0} = m_{\tilde{\chi}_2^0}$ ($m_{\tilde{\chi}_i^0} = m_{\tilde{\chi}_3^0}$) for $\tilde{\chi}_1^0 \tilde{\chi}_2^0$ ($\tilde{\chi}_1^0 \tilde{\chi}_3^0$) production.
- We apply the reconstruction procedure from App. A, assuming WW and slepton pair production. Thus, we calculate two values of y^2 , Eq. (A.9).
- The event solves the system of equations if

$$|\cos b| < 1 \quad \text{and} \quad |\cos B| < 1, \quad (17)$$

when neutralino production has been assumed, and

$$y^2 > 0, \quad (18)$$

when W /slepton production has been assumed.

⁷ The ambiguity is related to the neutralino momentum, for which we have two possible solutions

$$\mathbf{p}_{\tilde{\chi}_i^0} = \mathbf{p}_{\ell_N} + \mathbf{p}_{\tilde{\ell}} = \begin{pmatrix} |\mathbf{p}_{\tilde{\ell}}| \sin b \cos B \\ \pm |\mathbf{p}_{\tilde{\ell}}| \sin b \sin B \\ |\mathbf{p}_{\ell_N}| + |\mathbf{p}_{\tilde{\ell}}| \cos b \end{pmatrix}. \quad (16)$$

For this reason, the neutralino production plane cannot be resolved in $e^+e^- \rightarrow \tilde{\chi}_i^0 \tilde{\chi}_j^0$ processes for $j = 1$. For $j \geq 2$, the decay of $\tilde{\chi}_j^0$ could be included in order to reconstruct the production plane [58]. In that case larger triple product asymmetries can be studied, which include the neutralino momentum itself [35].

		system solved <i>only</i>				
		$\tilde{\chi}_1^0\tilde{\chi}_2^0$	$\tilde{\chi}_1^0\tilde{\chi}_3^0$	$\tilde{\ell}_R^+\tilde{\ell}_R^-$	W^+W^-	
true process	64 k	$\tilde{\chi}_1^0\tilde{\chi}_2^0$	41566	788	64	856
	74 k	$\tilde{\chi}_1^0\tilde{\chi}_3^0$	100	25513	369	873
	200 k	$\tilde{\ell}_R^+\tilde{\ell}_R^-$	181	1801	43919	3400
	8.8 k	W^+W^-	0	13	37	6802
		purity	99%	91%	99%	57%
		efficiency	65%	34%	22%	77%

Table 3: The numbers of leptonic events from the pair production of neutralinos, sleptons and W bosons, with their identification according to the kinematic selection procedure at the generator level, see Sec. 3.2. The events are simulated for our benchmark scenario, Tab. 1, with an integrated luminosity of $\mathcal{L} = 500 \text{ fb}^{-1}$ and beam polarization $(P_{e^-}, P_{e^+}) = (0.8, -0.6)$ for $\sqrt{s} = 500 \text{ GeV}$.

- The event is accepted and labeled as coming from a given process only if it solves *exactly one* out of the four above mentioned systems of equations, i.e. it fulfills condition (17) for $\tilde{\chi}_1^0\tilde{\chi}_2^0$ or $\tilde{\chi}_1^0\tilde{\chi}_3^0$ production, or condition (18) for W or slepton production.

In order to demonstrate the efficiency of this procedure we perform a Monte Carlo simulation of $\tilde{\chi}_1^0\tilde{\chi}_2^0$, $\tilde{\chi}_1^0\tilde{\chi}_3^0$, W^+W^- , and $\tilde{\ell}_R^+\tilde{\ell}_R^-$ production and their leptonic decays, using `Whizard 1.96` [70]. We use the MSSM parameters, Tab. 1, with an integrated luminosity of $\mathcal{L} = 500 \text{ fb}^{-1}$, and a beam polarization of $(P_{e^-}, P_{e^+}) = (0.8, -0.6)$ with realistic beam spectra⁸. In Tab. 3 the results of the event selection are summarized. Without any additional cuts, the selection method gives an excellent separation between the different samples at the MC level. This method is still performing well after a full detector simulation, as demonstrated in the following section.

The method can be successfully applied also for different particle mass spectra. In our benchmark scenario, due to the small difference between $\tilde{\ell}_R$ and $\tilde{\chi}_2^0$ masses, a separation of the near and far leptons, and of the $\tilde{\chi}_2^0$ and $\tilde{\chi}_3^0$ signals was rather straightforward, see Fig. 3. However, scenarios with different $m_{\tilde{\chi}_2^0} - m_{\tilde{\ell}_R}$ can turn out to be more demanding. In order to test the applicability of the kinematic reconstruction, we consider a scenario with $m_{\tilde{\ell}_R} = 146 \text{ GeV}$ and the other parameters kept as in the benchmark point. It can be regarded as the worst case scenario since the energies of leptons from neutralino $\tilde{\chi}_2^0$, $\tilde{\chi}_3^0$, and slepton decays are all in

⁸We include ISR and beamstrahlung, which slightly degrade the number of reconstructed events even if the correct process is assumed for a given event. Additionally, these effects will increase the number of false solutions, leading to wrong assignments.

the 10 to 80 GeV range. Therefore, in the kinematic reconstruction, one has to take into account two possible assignments of the near and far leptons. This, in principle, could result in a reduction of the efficiency. Nevertheless, in the case of $\tilde{\chi}_1^0\tilde{\chi}_3^0$ production the efficiency is about 40%. It drops to 8% for $\tilde{\chi}_1^0\tilde{\chi}_2^0$ pairs, since they likely also solve the kinematic on-shell conditions for the $\tilde{\chi}_1^0\tilde{\chi}_3^0$ production process. The purity, however, remains at about 90%. In half of the cases, one can also correctly and unambiguously assign near and far leptons.

4 Full detector simulation study

The next step of our analysis is passing the generated signal events and all relevant SM and SUSY background events through a full ILD simulation and event reconstruction. After discussing the preselection cuts for the leptonic event candidates, we apply the kinematic selection as described in the previous section.

4.1 Detector simulation and event reconstruction

For the present study we have performed a full simulation of the ILD detector designed for the ILC. A detailed description of the detector concept can be found in Ref. [71]. The ILD is a concept under study for a multipurpose particle detector with a forward-backward symmetric cylindrical geometry. It is designed for an excellent precision in momentum and energy measurements over a large solid angle. The tracking system consists of a multi-layer pixel-vertex detector, surrounded by a system of strip and pixel detectors and a large volume time projection chamber. The track finding efficiency is 99.5% for momenta above 1 GeV and angles down to $\theta = 7^\circ$, while the transverse momentum resolution is $\delta(1/p_T) \sim 2 \cdot 10^{-5} \text{ GeV}^{-1}$. The SiW electromagnetic calorimeter (ECAL) is highly segmented with a transverse cell size of $5 \text{ mm} \times 5 \text{ mm}$ and 20 layers. It provides an energy resolution of $(16.6 \pm 0.1)/\sqrt{E(\text{GeV})} \oplus (1.1 \pm 0.1)\%$ for the measurement of electrons and photons, and also the steel-scintillator hadronic calorimeter is highly granular and optimized for Particle Flow reconstruction. The calorimeters are surrounded by a large superconducting coil, creating an axial magnetic field of 3.5 Tesla.

For the simulation of the ILD, we use the *ILD_00* detector model, as implemented in the Geant4-based *Mokka* [72–74] package. We have taken into account all active elements, and also cables, cooling systems, support structures and dead regions. We have used the radiation hard beam calorimeter (BCAL) to reject forward $\gamma\gamma$ events at low angles. In particular the modeling of the response of the BCAL is relevant for the estimation of the background from events with activity in the very forward regions. This background was estimated by tracking electrons to the BCAL and determining the probability of detection from a map of the expected energy density from beamstrahlung pairs [75].

All relevant SM backgrounds⁹ and SUSY signal and background events are generated using *Whizard* [70], for $\mathcal{L} = 500 \text{ fb}^{-1}$ and $(P_{e^-}, P_{e^+}) = (0.8, -0.6)$. The

⁹We consider the final states listed in Tab. 5.

initial selection	no significant activity in BCAL number of all tracks $N_{\text{tracks}} \leq 7$
lepton selection	$\ell^+\ell^-$ pair with $\ell = e, \mu$ $ \cos\theta < 0.99$, min. energy $E > 3$ GeV lower energetic ℓ with $E < 18$ GeV, or higher energetic ℓ with $E > 38$ GeV higher energetic ℓ with $E \in [15, 150]$ GeV $\theta_{\text{acop}} > 0.2\pi$, $\theta_{\text{acol}} > 0.2\pi$
final preselection	$p_{\text{T}}^{\text{miss}} > 20$ GeV $E_{\text{vis}} < 150$ GeV $m_{\ell\ell} < 55$ GeV

Table 4: Preselection cuts, see Sec. 4.2 for details.

Whizard generator provides an ISR structure function that resums leading soft and collinear logarithms, and hard-collinear terms up to the third order [76]. The beamstrahlung is simulated using the **Circe** package [77]. After the detector simulation the events are reconstructed with **MarlinReco** [78]. We have used the Particle Flow concept, as it is implemented in **Pandora** [79].

4.2 Backgrounds and event preselection

In order to clearly measure the CP-violating effects in the production of neutralinos, we need to have a clean sample of signal events. Otherwise the CP asymmetry would be reduced by the CP-even backgrounds, which enter in the denominator, see Eq. (6). We therefore apply a number of preselection cuts listed in Tab. 4, to reject as much background as possible before applying the final selection.

4.2.1 Initial selection

For efficient electron and muon identification, we apply the following initial selection on the tracks and clusters reconstructed by the **Pandora** Particle Flow algorithm:

- $\frac{E_{\text{ECAL}}}{E_{\text{tot}}} > 0.6$ and $\frac{E_{\text{tot}}}{p_{\text{track}}} > 0.9$ for electrons;
- $\frac{E_{\text{ECAL}}}{E_{\text{tot}}} < 0.5$ and $\frac{E_{\text{tot}}}{p_{\text{track}}} < 0.3$ (0.8) for muons, with energy $E > (<) 12$ GeV,¹⁰

¹⁰The cut on the ratio of the total calorimeter energy and the track momentum is relaxed for low-energetic muons, which deposit more energy in the calorimeters. This ensures a reasonably high muon identification efficiency even for low-energetic muons.

where E_{ECAL} is the energy measured in the electromagnetic calorimeter, E_{tot} is the total measured energy in the calorimeters, and p_{track} is the measured track momentum in the tracking detectors. E is the energy of the Particle Flow object assigned by Pandora, which is derived from the track momentum in case a track is present or from the deposited energy in the calorimeters. We require no significant activity in the BCAL to reject $\gamma\gamma$ events. We select those events with less than eight tracks¹¹, $N_{\text{tracks}} \leq 7$, which efficiently removes all sorts of hadronic background.

4.2.2 Lepton selection

We require that two of the tracks form a pair of opposite-sign same-flavor leptons $\ell^+\ell^-$, with $\ell = e$ or μ . Only electrons or muons are selected with a polar angle $|\cos\theta| < 0.99$ and a minimum energy $E > 3$ GeV. There is a large contribution from beam induced $e^+e^- \rightarrow \gamma\gamma e^+e^- \rightarrow \ell\ell e^+e^-$ ($\ell = e, \mu, \tau$) background events¹² [71, 75]. The two outgoing beam electrons are high-energetic with a small scattering angle, while the rest of the event forms a system of low energy and mass. If the beam remnants escape close to the beam pipe, and cannot be rejected by a low angle veto, the missing transverse momentum of the event is limited, such that the remaining leptons are almost back-to-back in the transverse projection (T). Thus, we apply a cut on their acoplanarity angle

$$\theta_{\text{acop}} > 0.2\pi \quad \text{with} \quad \theta_{\text{acop}} = \pi - \arccos\left(\frac{\mathbf{p}_{\ell^+}^{\text{T}} \cdot \mathbf{p}_{\ell^-}^{\text{T}}}{|\mathbf{p}_{\ell^+}^{\text{T}}| |\mathbf{p}_{\ell^-}^{\text{T}}|}\right), \quad (19)$$

where $\theta_{\text{acop}} = 0$ for back-to-back (180°) events. Electrons or muons from $\gamma\gamma$ induced $\tau\tau$ events usually have energies below 10 GeV and can therefore be suppressed by exploiting that the far leptons from SUSY signal decays usually have higher energies. To do this and to select the signal lepton pairs $\ell^+\ell^-$ from the neutralino $\tilde{\chi}_{2,3}^0$ decays, we first use their energy distributions, see Fig. 3. We keep events where either the lower energetic lepton has $E < 18$ GeV, or the higher energetic lepton has $E > 38$ GeV. In addition the higher energetic lepton is required to have an energy $E \in [15, 150]$ GeV. Since the signal lepton pairs $\ell^+\ell^-$ originate from the same parent neutralino, they follow its direction in first approximation. The lepton pairs from SM decay processes, and also from slepton pair decays, tend to be more back-to-back, since the leptons originate from different mother particles. We therefore apply a cut on the acollinearity angle between the leptons

$$\theta_{\text{acol}} > 0.2\pi \quad \text{with} \quad \theta_{\text{acol}} = \pi - \arccos\left(\frac{\mathbf{p}_{\ell^+} \cdot \mathbf{p}_{\ell^-}}{|\mathbf{p}_{\ell^+}| |\mathbf{p}_{\ell^-}|}\right). \quad (20)$$

¹¹Although we expect to have only two isolated leptons in our signal events, we do not tighten this cut to avoid removing signal events due to overlaid $\gamma\gamma$ events.

¹²In this study we only consider the class of $\gamma\gamma$ background events where both photons from the e^+ and e^- beam interact via a virtual fermion. Interactions where the photon fluctuates into a vector-meson or where the photon is highly virtual and the interaction is best described as deep inelastic electron scattering on a vector-meson are not considered. Since their transverse momentum distributions are narrower, it is less likely that they contribute to the overall background [75, 80].

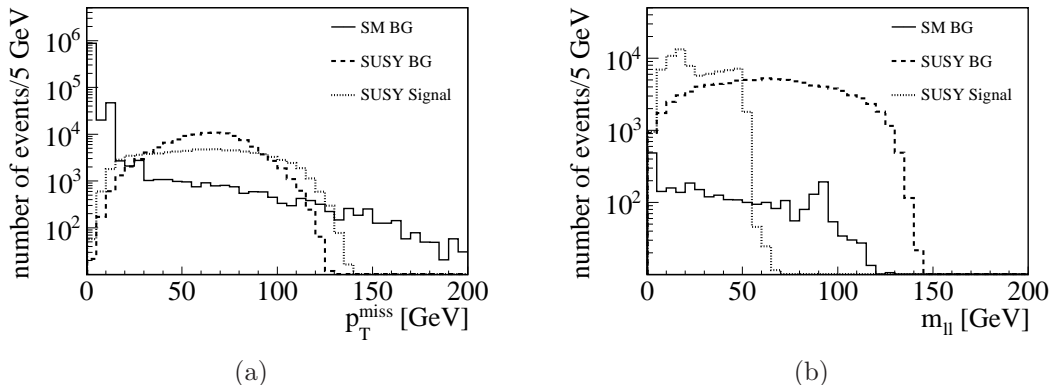


Figure 4: (a) Missing transverse momentum p_T^{miss} distribution of SM background, SUSY background and SUSY signal after the lepton selection, see Sec. 4.2.2. (b) Invariant mass $m_{\ell\ell}$ distribution of the lepton pair after all preselection cuts except the cut on $m_{\ell\ell}$. The events are simulated for $\mathcal{L} = 500 \text{ fb}^{-1}$, beam polarization $(P_{e^-}, P_{e^+}) = (0.8, -0.6)$ at $\sqrt{s} = 500 \text{ GeV}$, and MSSM parameters for our benchmark scenario, Tab. 1.

4.2.3 Final preselection

In Fig. 4(a), we show the missing transverse momentum, p_T^{miss} , distribution of the SM background, the SUSY background, and the SUSY signal after the lepton selection. The $\mathbf{p}_T^{\text{miss}}$ is calculated to balance out the sum of all reconstructed transverse particle momenta in an event. Our signal neutralinos $\tilde{\chi}_{2,3}^0$, but also the background sleptons, decay into the lightest neutralino, which escapes detection, thus giving signatures with high p_T^{miss} . However, most background lepton pairs from beam induced $\gamma\gamma$ events have a transverse momentum typically below 10 GeV, and are removed by the cut $p_T^{\text{miss}} > 20 \text{ GeV}$.¹³ Due to the escaping neutralinos, we also expect a limited total visible energy E_{vis} in the signal events, and we apply the cut $E_{\text{vis}} < 150 \text{ GeV}$. The visible energy is calculated as the sum of all reconstructed particle energies.

Finally we apply a cut $m_{\ell\ell} < 55 \text{ GeV}$ on the invariant mass of the lepton pair, see the distribution in Fig. 4(b), after all preselection cuts, except the cut on $m_{\ell\ell}$. The signal lepton pair from $\tilde{\chi}_3^0$ ($\tilde{\chi}_2^0$) decays has a sharp endpoint at 51 GeV (22 GeV), which is also exploited for mass measurements [81–83]. The invariant mass cut also removes SM backgrounds from ZZ and WW production. In Fig. 4(b), we can see the invariant mass peak of one of the Z bosons decaying into two electrons or muons, while the other decays into a neutrino pair. The WW events contribute to the background if they either both decay directly into same-flavor leptons, or if one of them decays into a τ , which in turn can complete the same-flavor lepton pair in the event by its subsequent decay.

The number of remaining events after the lepton selection and the entire event

¹³The spike in the 3rd bin of the p_T^{miss} distribution in Fig. 4(a) is due to $4 \gamma\gamma \rightarrow \ell\ell$ events that have a high event weight. Due to limited CPU time and the large cross section of these events, it is not possible to simulate an event sample corresponding to $\mathcal{L} = 500 \text{ fb}^{-1}$. The final preselection cuts are chosen such that this remaining high cross section background is safely removed.

class	final state	after lepton selection	after preselection
signal	$\tilde{\chi}_1^0 \tilde{\chi}_2^0 \rightarrow \tilde{\chi}_1^0 \tilde{\chi}_1^0 \ell \ell$ ($\ell \neq \tau$)	31543	28039
	$\tilde{\chi}_1^0 \tilde{\chi}_3^0 \rightarrow \tilde{\chi}_1^0 \tilde{\chi}_1^0 \ell \ell$ ($\ell \neq \tau$)	49084	45966
SUSY	$\tilde{\ell} \tilde{\ell} \rightarrow \tilde{\chi}_1^0 \tilde{\chi}_1^0 \ell \ell$ ($\ell \neq \tau$)	108302	34223
	$\tilde{\chi}_1^0 \tilde{\chi}_1^0 \tau \tau$	5147	4076
	$\tilde{\chi}_1^0 \tilde{\chi}_1^0 \ell \ell \nu \nu$	681	528
SM	$\ell \ell \nu \nu$	8241	1196
	$\tau \tau$	13017	360
	$\ell \ell$ ($\ell \neq \tau$)	24113	0
	qq	1380	0
	$\gamma \gamma$	917355	272

Table 5: Number of selected events after lepton selection and final preselection, for $\mathcal{L} = 500 \text{ fb}^{-1}$, $(P_{e^-}, P_{e^+}) = (0.8, -0.6)$ at $\sqrt{s} = 500 \text{ GeV}$. The MSSM parameters are given in Tab. 1.

preselection is listed in Tab. 5. The most severe remaining SM background stems from WW and ZZ production, while the slepton pair production is the dominant SUSY background. The difference in the numbers of selected $\tilde{\chi}_2^0$ and $\tilde{\chi}_3^0$ decays is due to different cross sections times branching ratios, see Tab. 2, and due to a reduced muon identification efficiency at low muon momenta, which reduces the efficiency for the selection of $\tilde{\chi}_2^0$ decays.

4.3 Signal identification with kinematic event selection

In order to measure our CP asymmetry from the preselected events, we now apply the kinematic selection procedure, which we have described for the signal in Sec. 3, and for the WW and $\tilde{\ell}\tilde{\ell}$ backgrounds in App. A. The kinematic selection allows us not only to reduce the remaining SUSY background from slepton pair production, but also to distinguish the lepton pairs which stem from $\tilde{\chi}_1^0 \tilde{\chi}_2^0$ or $\tilde{\chi}_1^0 \tilde{\chi}_3^0$ production and decay. This will be essential, since in our benchmark scenario, Tab. 1, the corresponding CP asymmetries have roughly equal size, but opposite sign, see Fig. 2.

For each preselected lepton pair, we require that it exclusively solves only one of the systems of equations, as discussed in Sec. 3.2. We reject all other events that solve more than one system of equations. In Tab. 4.3, we list the number of preselected events that fulfill this requirement. For the lepton pairs coming from $\tilde{\chi}_1^0 \tilde{\chi}_2^0$ decays, the final signal selection efficiency is 29%, and the total background contamination of the selected sample is about 8%. Lepton pairs from $\tilde{\chi}_1^0 \tilde{\chi}_3^0$ decays reach a signal selection efficiency of 27%, while the total background contamination of the selected sample is about 16%.

class	only $\tilde{\chi}_1^0\tilde{\chi}_2^0$	only $\tilde{\chi}_1^0\tilde{\chi}_3^0$	only $\tilde{\ell}_R^+\tilde{\ell}_R^-$	only W^+W^-
$\tilde{\chi}_1^0\tilde{\chi}_2^0 \rightarrow \tilde{\chi}_1^0\tilde{\chi}_1^0\ell\ell$ ($\ell \neq \tau$)	18343	615	51	855
$\tilde{\chi}_1^0\tilde{\chi}_3^0 \rightarrow \tilde{\chi}_1^0\tilde{\chi}_1^0\ell\ell$ ($\ell \neq \tau$)	290	20132	372	635
all SUSY background	1153	3055	5626	951
all SM background	87	256	44	81
purity	92%	84%	–	–
efficiency	29%	27%	–	–

Table 6: Number of preselected events from Tab. 5, that fulfill the requirements of the kinematic selection procedure, discussed in Sec. 4.3.

4.4 Measurement of the CP asymmetries

The CP asymmetries, Eq. (6), can now be calculated as the difference between the number of events N_+ and N_- , with the triple product $\mathcal{T} > 0$ or $\mathcal{T} < 0$, respectively,

$$\mathcal{A}(\mathcal{T}) = \frac{N_+ - N_-}{N_+ + N_-}. \quad (21)$$

We obtain

$$\mathcal{A}(\mathbf{p}_{e^-}, \mathbf{p}_{\ell_N^+}, \mathbf{p}_{\ell_F^-})_{\tilde{\chi}_1^0\tilde{\chi}_2^0} = -10.2 \pm 1.0\%, \quad (22)$$

$$\mathcal{A}(\mathbf{p}_{e^-}, \mathbf{p}_{\ell_N^-}, \mathbf{p}_{\ell_F^+})_{\tilde{\chi}_1^0\tilde{\chi}_2^0} = +10.7 \pm 1.0\%, \quad (23)$$

$$\mathcal{A}(\mathbf{p}_{e^-}, \mathbf{p}_{\ell_N^+}, \mathbf{p}_{\ell_F^-})_{\tilde{\chi}_1^0\tilde{\chi}_3^0} = +9.3 \pm 1.0\%, \quad (24)$$

$$\mathcal{A}(\mathbf{p}_{e^-}, \mathbf{p}_{\ell_N^-}, \mathbf{p}_{\ell_F^+})_{\tilde{\chi}_1^0\tilde{\chi}_3^0} = -8.8 \pm 1.0\%, \quad (25)$$

with the statistical uncertainty [84]

$$\delta(\mathcal{A})_{\text{stat}} = \sqrt{\frac{1 - \mathcal{A}^2}{N}}, \quad (26)$$

and the total number of events $N = N_+ + N_-$. Exchanging the near and far leptons gives, within the uncertainties, the same size of the asymmetry but with opposite sign, see Eq. (7). However, the values of the asymmetries are different from the theoretical values, see Tab. 2, which is mainly due to:

1. CP-even background events cancel in the numerator, but contribute to the denominator in Eq. (21).
2. Events are removed by the experimental selection cuts and by the kinematic selection procedure, which can bias the measured asymmetry.

CP-even backgrounds shift the asymmetry to slightly lower values, whereas the selection cuts have the opposite effect. If we assume that the background contributions

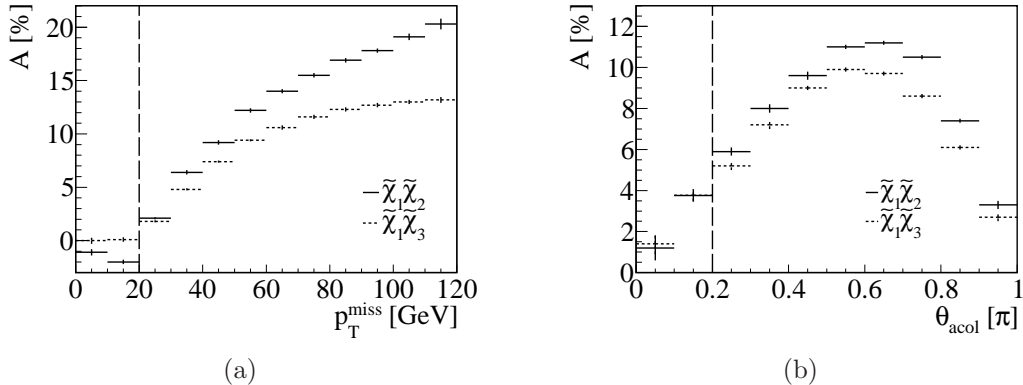


Figure 5: The (a) $\mathbf{p}_T^{\text{miss}}$ and (b) θ_{acol} dependence of the asymmetries $\mathcal{A}(\mathbf{p}_{e^-}, \mathbf{p}_{\ell_N^-}, \mathbf{p}_{\ell_F^+})_{\tilde{\chi}_1^0 \tilde{\chi}_2^0}$ and $\mathcal{A}(\mathbf{p}_{e^-}, \mathbf{p}_{\ell_N^-}, \mathbf{p}_{\ell_F^-})_{\tilde{\chi}_1^0 \tilde{\chi}_3^0}$, solid and dashed lines, respectively. The cut value used in our analysis is indicated by the dashed line. In each case 10^7 events were generated and no detector effects are included. Statistical uncertainties are shown.

are known, we obtain

$$\mathcal{A}(\mathbf{p}_{e^-}, \mathbf{p}_{\ell_N^+}, \mathbf{p}_{\ell_F^-})_{\tilde{\chi}_1^0 \tilde{\chi}_2^0} = -11.0 \pm 1.0\%, \quad (27)$$

$$\mathcal{A}(\mathbf{p}_{e^-}, \mathbf{p}_{\ell_N^-}, \mathbf{p}_{\ell_F^+})_{\tilde{\chi}_1^0 \tilde{\chi}_2^0} = +11.6 \pm 1.0\%, \quad (28)$$

$$\mathcal{A}(\mathbf{p}_{e^-}, \mathbf{p}_{\ell_N^+}, \mathbf{p}_{\ell_F^-})_{\tilde{\chi}_1^0 \tilde{\chi}_3^0} = +11.1 \pm 1.0\%, \quad (29)$$

$$\mathcal{A}(\mathbf{p}_{e^-}, \mathbf{p}_{\ell_N^-}, \mathbf{p}_{\ell_F^+})_{\tilde{\chi}_1^0 \tilde{\chi}_3^0} = -10.6 \pm 1.0\%. \quad (30)$$

Additionally, we have studied the bias due to the selection procedure by calculating the asymmetry after each cut and comparing the results obtained from `Whizard` with the results obtained from `Herwig++` [85–87]. Both programs show consistently a total shift of about 2% towards larger values after the application of the complete selection procedure; see also Ref. [27]. The cuts remove events with a small value of the asymmetry inducing an upward shift. As an example, Fig. 5 shows the dependence of the asymmetry on $\mathbf{p}_T^{\text{miss}}$ and θ_{acol} , indicating also our cut value. The shift will be taken into account in the parameter fit described in the next section.

5 Fit of the parameters in the neutralino sector

In the final step of our analysis, we estimate the accuracy to determine the parameters in the neutralino sector of the MSSM. These are the six free parameters of the neutralino mass matrix, see App. B,

$$|M_1|, \quad M_2, \quad |\mu|, \quad \tan\beta, \quad \phi_1, \quad \phi_\mu. \quad (31)$$

We have a number of observables at hand that can be used in the fit. These are cross sections, masses, and asymmetries. Masses will be measured with high precision using different methods [34]. For the neutralino masses we assume the uncertainties

as in Ref. [84], since no detailed analysis has been done for our parameter point. However, these uncertainties are rather conservative, since we expect that in our scenario a similar precision can be achieved as in [88]. In case of the cross sections, the uncertainty is dominated by the statistical uncertainty,

$$\frac{\Delta\sigma}{\sigma} = \frac{\sqrt{S+B}}{S}, \quad (32)$$

where S and B are the signal and background contributions, respectively; see Tab. 5. Since experimentally the number of events is recorded, not the cross section itself, we have to take into account branching ratios for the relevant decays. These will depend on the masses and, in case of staus, on the stau mixing angle, $\cos\theta_{\tilde{\tau}}$. The stau mixing angle can be obtained from τ polarization measurements in stau pair production [75], with an accuracy of 5% [89–91].

After our procedure of the kinematic event selection, see Sec. 4.3, to disentangle contributions from $\tilde{\chi}_1^0\tilde{\chi}_2^0$ and $\tilde{\chi}_1^0\tilde{\chi}_3^0$ production and decay, the background contributions are below 15%. The small uncertainties in the beam polarizations of 0.5% [56], in the luminosity, and in the SUSY masses are negligible, see also Ref. [81–83]. For the CP asymmetries, we have estimated relative uncertainties of the order of 10% in Sec. 4.4. For the fit we take into account a bias due to cuts on the asymmetry derived from the MC simulation, as described in Sec. 4.4. Thus, the analytical value of the asymmetry, given in Tab. 2, is shifted accordingly. Furthermore, we use Eq. (8) to calculate the measured value of the asymmetry, which is free of FSI effects. In summary, we have the following set of input observables and uncertainties:

$$\begin{aligned} m_{\tilde{\chi}_1^0} &= 117.3 \pm 0.2 \text{ GeV}, \\ m_{\tilde{\chi}_2^0} &= 168.5 \pm 0.5 \text{ GeV}, \\ m_{\tilde{\chi}_3^0} &= 180.8 \pm 0.5 \text{ GeV}, \\ \sigma(\tilde{\chi}_1^0\tilde{\chi}_2^0) \times \text{BR}(\tilde{\chi}_2^0 \rightarrow \tilde{\ell}_R\ell) &= 130.9 \pm 1.4 \text{ fb}, \\ \sigma(\tilde{\chi}_1^0\tilde{\chi}_3^0) \times \text{BR}(\tilde{\chi}_3^0 \rightarrow \tilde{\ell}_R\ell) &= 155.7 \pm 1.6 \text{ fb}, \\ \sigma(\tilde{\chi}_2^0\tilde{\chi}_2^0) \times \text{BR}(\tilde{\chi}_2^0 \rightarrow \tilde{\ell}_R\ell)^2 &= 4.8 \pm 0.3 \text{ fb}, \\ \sigma(\tilde{\chi}_3^0\tilde{\chi}_3^0) \times \text{BR}(\tilde{\chi}_3^0 \rightarrow \tilde{\ell}_R\ell)^2 &= 26.3 \pm 0.7 \text{ fb}, \\ \sigma(\tilde{\chi}_2^0\tilde{\chi}_3^0) \times \text{BR}(\tilde{\chi}_2^0 \rightarrow \tilde{\ell}_R\ell) \times \text{BR}(\tilde{\chi}_3^0 \rightarrow \tilde{\ell}_R\ell) &= 28.9 \pm 0.7 \text{ fb}, \\ \mathcal{A}^{\text{CP}}(\mathbf{p}_{e^-}, \mathbf{p}_{\ell_N}, \mathbf{p}_{\ell_F})_{\tilde{\chi}_1^0\tilde{\chi}_2^0} &= +11.3\% \pm 0.7\%, \\ \mathcal{A}^{\text{CP}}(\mathbf{p}_{e^-}, \mathbf{p}_{\ell_N}, \mathbf{p}_{\ell_F})_{\tilde{\chi}_1^0\tilde{\chi}_3^0} &= -10.9\% \pm 0.7\%. \end{aligned}$$

The uncertainties for the cross sections correspond to an integrated luminosity of $\mathcal{L} = 500 \text{ fb}^{-1}$. We perform a six dimensional χ^2 fit using `Minuit` [92, 93]

$$\chi^2 = \sum_i \left| \frac{\mathcal{O}_i - \bar{\mathcal{O}}_i}{\delta\mathcal{O}_i} \right|^2, \quad (33)$$

where the sum runs over the input observables \mathcal{O}_i mentioned above, with their corresponding experimental uncertainties $\delta\mathcal{O}_i$. The theoretical values calculated using the fitted MSSM parameters, Eq. (31), are denoted by $\bar{\mathcal{O}}_i$. The parameter

dependence of branching ratios (e.g. the stau mixing angle) is also included in the fit, but has negligible impact. We then obtain the following fitted values for the MSSM parameters:

$$\begin{aligned}
|M_1| &= 150.0 \pm 0.7 \text{ GeV}, \\
M_2 &= 300 \pm 5 \text{ GeV}, \\
|\mu| &= 165.0 \pm 0.3 \text{ GeV}, \\
\tan \beta &= 10.0 \pm 1.6, \\
\phi_1 &= 0.63 \pm 0.05, \\
\phi_\mu &= 0.0 \pm 0.2.
\end{aligned}$$

The best estimates are obtained for the $|M_1|$ and $|\mu|$ mass parameters, since the neutralino states $\tilde{\chi}_1^0$, $\tilde{\chi}_2^0$, and $\tilde{\chi}_3^0$ are mostly composed of bino and Higgsino. The fourth neutralino is heavy and cannot be measured, so the limit on the wino mass M_2 is not as good. Also a rather large uncertainty is obtained for $\tan \beta$. However, if additional measurements from other sectors will be added, it should be improved significantly. We note that the precision obtained in this study is similar to the results of Ref. [83], which uses a similar set of observables.¹⁴

It is remarkable that the moduli of the phases ϕ_1 and ϕ_μ can also be determined with high precision, using the CP-even observables alone. However, only an inclusion of CP-odd asymmetries in the fit allows us to resolve the sign ambiguities of the phases. Without the CP-odd asymmetries in the fit we would have a twofold ambiguity, $\phi_1 = \pm 0.6$, and even fourfold if $\phi_\mu \neq 0$. Thus, the triple product asymmetries are not only a direct test of CP violation, but are also essential to determine the correct values of the phases.

6 Summary and conclusions

We have presented the first full detector simulation study to measure SUSY CP phases at the ILC. We have considered CP-sensitive triple-product asymmetries in neutralino production $e^+e^- \rightarrow \tilde{\chi}_i^0 \tilde{\chi}_1^0$ and the subsequent leptonic two-body decay chain $\tilde{\chi}_i^0 \rightarrow \tilde{\ell}_R \ell$, $\tilde{\ell}_R \rightarrow \tilde{\chi}_1^0 \ell$, for $\ell = e, \mu$. Large asymmetries typically arise due to strong neutralino mixing. This causes on the one side that asymmetries for $\tilde{\chi}_1^0 \tilde{\chi}_2^0$ and $\tilde{\chi}_1^0 \tilde{\chi}_3^0$ production have about the same size but opposite sign. On the other side the strong mixing implies two close-in-mass neutralino states, that can have a mass separation of the order of 10 GeV. This quasi-degeneracy would potentially pose a problem for the separation of both signal components.

Therefore we have developed a kinematic selection method, to identify the lepton pairs from the signal events. At the Monte Carlo level, we have shown that this

¹⁴The high precision achieved in the fit calls for the inclusion of higher order corrections which can be in the $\mathcal{O}(20\%)$ regime in the neutralino system, see e.g. [94, 95]. These corrections will in turn depend on the full parameter set of the MSSM. Therefore, the proper treatment would require the inclusion of observables from other sectors, in particular from the third generation of squarks, cf. Ref. [96, 97]. This issue is beyond the scope of this paper, however, it should stimulate further studies.

method allows one to separate the leptons from the two signal processes $\tilde{\chi}_1^0\tilde{\chi}_2^0$ and $\tilde{\chi}_1^0\tilde{\chi}_3^0$, and also to reduce the major SM and SUSY backgrounds, in particular from W -pair and slepton-pair production.

Then we have performed a detailed case study, which includes a full ILD detector simulation and event reconstruction. A detailed cut flow analysis has been done to preselect leptonic event candidates, which then have been passed to our method of kinematic selection. Even after the detector simulation, our method has worked efficiently to reduce background and separate the signal. After the full simulation with kinematic selection, the efficiencies of signal event selection is of the order of 27% with a purity of about 90% of the event samples. That allows one to measure the asymmetry with a relative precision of about 10%. Our method of kinematic event reconstruction also works well in scenarios with different mass splittings of the neutralinos and the selectron. In the worst case scenario we found that the efficiency will go down to some 10%, but still with a high purity of the correctly identified signal sample of the order of 90%.

We have performed a global fit of the neutralino masses, cross sections, and CP asymmetries to reconstruct the MSSM parameters of the neutralino sector, including the CP phases. The relative uncertainties of the parameters $|M_1|$ and $|\mu|$ are below 1%, those for M_2 about 1%, and for $\tan\beta$ and the CP phases ϕ_1, ϕ_μ about 10%. Although the moduli of the phases ϕ_1, ϕ_μ can also be determined by using the CP-even observables alone, we have shown that only an inclusion of CP-odd asymmetries in the fit allows us to resolve the sign ambiguities of the phases.

To summarize, we have shown that a measurement of the neutralino sector seems to be feasible, including CP phases. In particular the triple product asymmetries are not only a direct test of CP violation, but are also essential to determine the correct values of the phases in the neutralino sector.

Acknowledgments

We would like to thank Steve Aplin, Mikael Berggren, Jan Engels, Frank Gaede, Nina Herder, Jenny List, and Mark Thomson for useful discussions and help with the detector simulations. This work was supported by MICINN project FPA.2006-05294 and CPAN. We acknowledge the support of the DFG through the SFB (grant SFB 676/1-2006).

A Reconstruction of W and $\tilde{\ell}$ pair production

We consider a template process

$$e^+ + e^- \rightarrow A + \bar{A} \rightarrow \ell + \bar{\ell} + B + B, \quad (\text{A.1})$$

where $(A, B) = (\tilde{\ell}, \tilde{\chi}_1^0)$ or (W, ν) . In both cases $B = \tilde{\chi}_1^0$ or ν escapes detection. Since the system of the lepton pair has to obey different kinematic constraints, we

consider the question, whether the final lepton pair can be assigned to its mother production process, if the lepton momenta are measured, and the slepton and LSP masses are known. We follow closely Ref. [69], and define the notation

$$c_1 \equiv \mathbf{p}_A \cdot \mathbf{p}_\ell = \frac{1}{2}(m_B^2 - m_A^2 + E_\ell \sqrt{s}), \quad (\text{A.2})$$

$$c_2 \equiv \mathbf{p}_A \cdot \mathbf{p}_{\bar{\ell}} = -\frac{1}{2}(m_B^2 - m_A^2 + E_{\bar{\ell}} \sqrt{s}), \quad (\text{A.3})$$

$$b_2 \equiv \mathbf{p}_A \cdot \mathbf{p}_A = \frac{s}{4} - m_A^2, \quad (\text{A.4})$$

$$a_{11} \equiv \mathbf{p}_\ell \cdot \mathbf{p}_\ell, \quad a_{12} \equiv \mathbf{p}_\ell \cdot \mathbf{p}_{\bar{\ell}}, \quad a_{22} \equiv \mathbf{p}_{\bar{\ell}} \cdot \mathbf{p}_{\bar{\ell}}. \quad (\text{A.5})$$

The momentum \mathbf{p}_A can be decomposed into the final lepton momenta

$$\mathbf{p}_A = t_1 \mathbf{p}_\ell + t_2 \mathbf{p}_{\bar{\ell}} + y \mathbf{p}_\perp, \quad (\text{A.6})$$

where $\mathbf{p}_\perp = \mathbf{p}_\ell \times \mathbf{p}_{\bar{\ell}}$. The expansion coefficients follow from Eqs. (A.2) and (A.3)

$$\left| \begin{array}{l} c_1 = t_1 a_{11} + t_2 a_{12} \\ c_2 = t_1 a_{12} + t_2 a_{22} \end{array} \right| \Rightarrow \left| \begin{array}{l} t_1 = \frac{a_{22} c_1 - a_{12} c_2}{a_{11} a_{22} - a_{12}^2} \\ t_2 = \frac{a_{11} c_2 - a_{12} c_1}{a_{11} a_{22} - a_{12}^2} \end{array} \right|. \quad (\text{A.7})$$

We finally obtain, from Eqs. (A.4) and (A.7),

$$b_2 = (t_1^2 a_{11} + 2t_1 t_2 a_{12} + t_2^2 a_{22}) + y^2 |\mathbf{p}_\perp|^2, \quad (\text{A.8})$$

$$\Rightarrow y^2 = \frac{b_2 - (t_1^2 a_{11} + 2t_1 t_2 a_{12} + t_2^2 a_{22})}{|\mathbf{p}_\perp|^2}. \quad (\text{A.9})$$

The equation for y constitutes a condition for existence of physical solutions of the system, i.e. $y^2 \geq 0$, where y^2 is computed from the kinematic variables s , m_A , m_B , E_ℓ , $E_{\bar{\ell}}$, and $\mathbf{p}_\ell \cdot \mathbf{p}_{\bar{\ell}}$. Similar to neutralino pair production, Sec. 3.1, Eq. (16), there remains a twofold ambiguity in solving the W or $\tilde{\ell}$ system, $y = \pm \sqrt{y^2}$.

B Neutralino mixing

The complex symmetric mass matrix of the neutralinos in the photino, zino, Higgsino basis $(\tilde{\gamma}, \tilde{Z}, \tilde{H}_a^0, \tilde{H}_b^0)$, is given by [66]

$$\mathcal{M}_{\chi^0} = \begin{pmatrix} M_2 s_W^2 + M_1 c_W^2 & (M_2 - M_1) s_W c_W & 0 & 0 \\ (M_2 - M_1) s_W c_W & M_2 c_W^2 + M_1 s_W^2 & m_Z & 0 \\ 0 & m_Z & \mu s_{2\beta} & -\mu c_{2\beta} \\ 0 & 0 & -\mu c_{2\beta} & -\mu s_{2\beta} \end{pmatrix}, \quad (\text{B.1})$$

with the short hand notation for the angles $s_W = \sin \theta_W$, $c_W = \cos \theta_W$, and $s_{2\beta} = \sin(2\beta)$, $c_{2\beta} = \cos(2\beta)$, and the $SU(2)$ gaugino mass parameter M_2 . The phases of the complex parameters $M_1 = |M_1| e^{i\phi_1}$ and $\mu = |\mu| e^{i\phi_\mu}$ can lead to CP-violating

effects in the neutralino system. The phase of M_2 can be rotated away by a suitable redefinition of the fields. We diagonalize the neutralino mass matrix with a complex, unitary 4×4 matrix N ,

$$N^* \cdot \mathcal{M}_{\chi^0} \cdot N^\dagger = \text{diag}(m_{\chi_1^0}, \dots, m_{\chi_4^0}), \quad (\text{B.2})$$

with the real neutralino masses $0 < m_{\chi_1^0} < m_{\chi_2^0} < m_{\chi_3^0} < m_{\chi_4^0}$.

References

- [1] H. E. Haber and G. L. Kane, *Phys. Rept.* **117** (1985) 75–263.
- [2] H. P. Nilles, *Phys. Rept.* **110** (1984) 1–162.
- [3] H. E. Haber, *Nucl. Phys. Proc. Suppl.* **62** (1998) 469–484, [arXiv:hep-ph/9709450](#).
- [4] T. Ibrahim and P. Nath, [arXiv:hep-ph/0210251](#).
- [5] T. Ibrahim and P. Nath, *Rev. Mod. Phys.* **80** (2008) 577–631, [arXiv:0705.2008 \[hep-ph\]](#).
- [6] J. R. Ellis, J. S. Lee, and A. Pilaftsis, *Phys. Rev.* **D76** (2007) 115011, [arXiv:0708.2079 \[hep-ph\]](#).
- [7] V. D. Barger *et al.*, *Phys. Rev.* **D64** (2001) 056007, [arXiv:hep-ph/0101106](#).
- [8] J. R. Ellis, S. Ferrara, and D. V. Nanopoulos, *Phys. Lett.* **B114** (1982) 231.
- [9] A. Bartl, W. Majerotto, W. Porod, and D. Wyler, *Phys. Rev.* **D68** (2003) 053005, [arXiv:hep-ph/0306050](#).
- [10] S. Y. Choi, M. Drees, and B. Gaissmaier, *Phys. Rev.* **D70** (2004) 014010, [arXiv:hep-ph/0403054](#).
- [11] S. Yaser Ayazi and Y. Farzan, *Phys. Rev.* **D74** (2006) 055008, [arXiv:hep-ph/0605272](#).
- [12] J. R. Ellis, J. S. Lee, and A. Pilaftsis, *JHEP* **10** (2008) 049, [arXiv:0808.1819 \[hep-ph\]](#).
- [13] F. Deppisch and O. Kittel, *JHEP* **09** (2009) 110, [arXiv:0905.3088 \[hep-ph\]](#).
- [14] A. Bartl, S. Hesselbach, K. Hidaka, T. Kernreiter, and W. Porod, *Phys. Lett.* **B573** (2003) 153–161, [arXiv:hep-ph/0307317](#).
- [15] A. Bartl, S. Hesselbach, K. Hidaka, T. Kernreiter, and W. Porod, *Phys. Rev.* **D70** (2004) 035003, [arXiv:hep-ph/0311338](#).

- [16] A. Bartl, K. Hidaka, T. Kernreiter, and W. Porod, *Phys. Lett.* **B538** (2002) 137–145, [arXiv:hep-ph/0204071](#).
- [17] A. Bartl, K. Hidaka, T. Kernreiter, and W. Porod, *Phys. Rev.* **D66** (2002) 115009, [arXiv:hep-ph/0207186](#).
- [18] K. Rolbiecki, J. Tattersall, and G. Moortgat-Pick, *Eur. Phys. J.* **C71** (2011) 1517, [arXiv:0909.3196 \[hep-ph\]](#).
- [19] T. Gajdosik, R. M. Godbole, and S. Kraml, *JHEP* **09** (2004) 051, [arXiv:hep-ph/0405167](#).
- [20] G. Valencia, [arXiv:hep-ph/9411441](#).
- [21] G. C. Branco, L. Lavoura, and J. P. Silva, *Int. Ser. Monogr. Phys.* **103** (1999) 1–536.
- [22] A. Bartl, H. Fraas, T. Kernreiter, and O. Kittel, *Eur. Phys. J.* **C33** (2004) 433–442, [arXiv:hep-ph/0306304](#).
- [23] P. Langacker, G. Paz, L.-T. Wang, and I. Yavin, *JHEP* **07** (2007) 055, [arXiv:hep-ph/0702068](#).
- [24] G. Moortgat-Pick, K. Rolbiecki, J. Tattersall, and P. Wienemann, *JHEP* **01** (2010) 004, [arXiv:0908.2631 \[hep-ph\]](#).
- [25] A. Bartl, E. Christova, K. Hohenwarter-Sodek, and T. Kernreiter, *Phys. Rev.* **D70** (2004) 095007, [arXiv:hep-ph/0409060](#).
- [26] J. Ellis, F. Moortgat, G. Moortgat-Pick, J. M. Smillie, and J. Tattersall, *Eur. Phys. J.* **C60** (2009) 633–651, [arXiv:0809.1607 \[hep-ph\]](#).
- [27] G. Moortgat-Pick, K. Rolbiecki, and J. Tattersall, *Phys. Rev.* **D83** (2011) 115012, [arXiv:1008.2206 \[hep-ph\]](#).
- [28] A. Bartl, E. Christova, K. Hohenwarter-Sodek, and T. Kernreiter, *JHEP* **11** (2006) 076, [arXiv:hep-ph/0610234](#).
- [29] F. F. Deppisch and O. Kittel, *JHEP* **06** (2010) 067, [arXiv:1003.5186 \[hep-ph\]](#).
- [30] H. Dreiner, O. Kittel, S. Kulkarni, and A. Marold, *Phys. Rev.* **D83** (2011) 095012, [arXiv:1011.2449 \[hep-ph\]](#).
- [31] **ILC** Collaboration, T. Behnke, (Ed.) *et al.*, [arXiv:0712.2356 \[physics.ins-det\]](#).
- [32] **ILC** Collaboration, J. Brau, (Ed.) *et al.*, [arXiv:0712.1950 \[physics.acc-ph\]](#).
- [33] **ILC** Collaboration, G. Aarons *et al.*, [arXiv:0709.1893 \[hep-ph\]](#).

- [34] **ECFA/DESY LC Physics Working Group** Collaboration, J. A. Aguilar-Saavedra *et al.*, [arXiv:hep-ph/0106315](#).
- [35] A. Bartl, H. Fraas, O. Kittel, and W. Majerotto, *Phys. Rev.* **D69** (2004) 035007, [arXiv:hep-ph/0308141](#).
- [36] A. Bartl, T. Kernreiter, and O. Kittel, *Phys. Lett.* **B578** (2004) 341–348, [arXiv:hep-ph/0309340](#).
- [37] S. Y. Choi, M. Drees, B. Gaissmaier, and J. Song, *Phys. Rev.* **D69** (2004) 035008, [arXiv:hep-ph/0310284](#).
- [38] A. Bartl, H. Fraas, O. Kittel, and W. Majerotto, *Eur. Phys. J.* **C36** (2004) 233–243, [arXiv:hep-ph/0402016](#).
- [39] J. A. Aguilar-Saavedra, *Nucl. Phys.* **B697** (2004) 207–224, [arXiv:hep-ph/0404104](#).
- [40] S. Y. Choi and Y. G. Kim, *Phys. Rev.* **D69** (2004) 015011, [arXiv:hep-ph/0311037](#).
- [41] A. Bartl, K. Hohenwarter-Sodek, T. Kernreiter, O. Kittel, and M. Terwort, *JHEP* **07** (2009) 054, [arXiv:0905.1782 \[hep-ph\]](#).
- [42] O. Kittel, [arXiv:hep-ph/0504183](#).
- [43] Y. Kizukuri and N. Oshimo, *Phys. Lett.* **B249** (1990) 449–454.
- [44] S. Y. Choi, H. S. Song, and W. Y. Song, *Phys. Rev.* **D61** (2000) 075004, [arXiv:hep-ph/9907474](#).
- [45] A. Bartl, H. Fraas, S. Hesselbach, K. Hohenwarter-Sodek, and G. A. Moortgat-Pick, *JHEP* **08** (2004) 038, [arXiv:hep-ph/0406190](#).
- [46] J. A. Aguilar-Saavedra, *Phys. Lett.* **B596** (2004) 247–255, [arXiv:hep-ph/0403243](#).
- [47] S. Y. Choi, B. C. Chung, J. Kalinowski, Y. G. Kim, and K. Rolbiecki, *Eur. Phys. J.* **C46** (2006) 511–520, [arXiv:hep-ph/0504122](#).
- [48] S. Y. Choi *et al.*, *Eur. Phys. J.* **C14** (2000) 535–546, [arXiv:hep-ph/0002033](#).
- [49] A. Bartl, H. Fraas, O. Kittel, and W. Majerotto, *Phys. Lett.* **B598** (2004) 76–82, [arXiv:hep-ph/0406309](#).
- [50] O. Kittel, A. Bartl, H. Fraas, and W. Majerotto, *Phys. Rev.* **D70** (2004) 115005, [arXiv:hep-ph/0410054](#).
- [51] J. A. Aguilar-Saavedra, *Nucl. Phys.* **B717** (2005) 119–136, [arXiv:hep-ph/0410068](#).

- [52] A. Bartl, K. Hohenwarter-Sodek, T. Kernreiter, O. Kittel, and M. Terwort, *Nucl. Phys.* **B802** (2008) 77–91, [arXiv:0802.3592 \[hep-ph\]](#).
- [53] H. K. Dreiner, O. Kittel, and A. Marold, *Phys. Rev.* **D82** (2010) 116005, [arXiv:1001.4714 \[hep-ph\]](#).
- [54] Y. Kizukuri and N. Oshimo, [arXiv:hep-ph/9310224](#).
- [55] A. Bartl *et al.*, *Eur. Phys. J.* **C51** (2007) 149–161, [arXiv:hep-ph/0608065](#).
- [56] G. Moortgat-Pick *et al.*, *Phys. Rept.* **460** (2008) 131–243, [arXiv:hep-ph/0507011](#).
- [57] A. Bartl, K. Hohenwarter-Sodek, T. Kernreiter, and H. Rud, *Eur. Phys. J.* **C36** (2004) 515–522, [arXiv:hep-ph/0403265](#).
- [58] A. Bartl *et al.*, *JHEP* **01** (2006) 170, [arXiv:hep-ph/0510029](#).
- [59] S. Y. Choi, M. Drees, and J. Song, *JHEP* **09** (2006) 064, [arXiv:hep-ph/0602131](#).
- [60] A. Bartl *et al.*, *Phys. Lett.* **B644** (2007) 165–171, [arXiv:hep-ph/0610431](#).
- [61] A. Bartl, K. Hohenwarter-Sodek, T. Kernreiter, and O. Kittel, *JHEP* **09** (2007) 079, [arXiv:0706.3822 \[hep-ph\]](#).
- [62] J. A. Aguilar-Saavedra and A. M. Teixeira, *Nucl. Phys.* **B675** (2003) 70–98, [arXiv:hep-ph/0307001](#).
- [63] J. A. Aguilar-Saavedra, [arXiv:hep-ph/0312140](#).
- [64] M. Berggren, [arXiv:hep-ph/0508247 \[hep-ph\]](#).
- [65] D. Atwood, S. Bar-Shalom, G. Eilam, and A. Soni, *Phys. Rept.* **347** (2001) 1–222, [arXiv:hep-ph/0006032](#).
- [66] S. Y. Choi, J. Kalinowski, G. A. Moortgat-Pick, and P. M. Zerwas, *Eur. Phys. J.* **C22** (2001) 563–579, [arXiv:hep-ph/0108117](#). Addendum-*ibid.* **C 23** (2002) 769.
- [67] G. A. Moortgat-Pick, H. Fraas, A. Bartl, and W. Majerotto, *Eur. Phys. J.* **C9** (1999) 521–534, [arXiv:hep-ph/9903220](#). Erratum-*ibid.* **C 9** (1999) 549.
- [68] J. Bernabéu and M. B. Gavela in *CP Violation*, C. Jarlskog, ed., p. 269. World Scientific, Singapore, 1989.
- [69] M. R. Buckley, H. Murayama, W. Klemm, and V. Rentala, *Phys. Rev.* **D78** (2008) 014028, [arXiv:0711.0364 \[hep-ph\]](#).
- [70] W. Kilian, T. Ohl, and J. Reuter, [arXiv:0708.4233 \[hep-ph\]](#).

- [71] ILD Concept Group, [arXiv:1006.3396](https://arxiv.org/abs/1006.3396) [hep-ex].
- [72] **GEANT4** Collaboration, S. Agostinelli *et al.*, *Nucl. Instrum. Meth.* **A506** (2003) 250–303.
- [73] G. Musat, *LCWS 2004, Proceedings* (2004) 437–439.
- [74] P. Mora de Freitas, *LCWS 2004, Proceedings* (2004) 441–444.
- [75] P. Bechtle, M. Berggren, J. List, P. Schade, and O. Stempel, *Phys. Rev.* **D82** (2010) 055016, [arXiv:0908.0876](https://arxiv.org/abs/0908.0876) [hep-ex].
- [76] M. Skrzypek and S. Jadach, *Z.Phys.* **C49** (1991) 577–584.
- [77] T. Ohl, *Comput.Phys.Commun.* **101** (1997) 269–288, [arXiv:hep-ph/9607454](https://arxiv.org/abs/hep-ph/9607454) [hep-ph].
- [78] O. Wendt, F. Gaede, and T. Kramer, *Pramana* **69** (2007) 1109–1114, [arXiv:physics/0702171](https://arxiv.org/abs/physics/0702171) [PHYSICS].
- [79] M. A. Thomson, *AIP Conf. Proc.* **896** (2007) 215–224.
- [80] P. Bambade, M. Berggren, F. Richard, and Z. Zhang, [arXiv:hep-ph/0406010](https://arxiv.org/abs/hep-ph/0406010) [hep-ph].
- [81] M. Ball, *Rekonstruktion von Neutralinos mit TESLA*, Diplomarbeit, University of Hamburg, 2003, <http://www-flc.desy.de/thesis/diplom.2002.ball.ps.gz>.
- [82] N. D’Ascenzo, *Study of the neutralino sector and analysis of the muon response of a highly granular hadron calorimeter at the International Linear Collider*, PhD thesis, DESY, Hamburg, 2009, <http://www-library.desy.de/cgi-bin/showprep.pl?desy-thesis-09-004>.
- [83] K. Desch, J. Kalinowski, G. A. Moortgat-Pick, M. M. Nojiri, and G. Polesello, *JHEP* **02** (2004) 035, [arXiv:hep-ph/0312069](https://arxiv.org/abs/hep-ph/0312069).
- [84] K. Desch, J. Kalinowski, G. Moortgat-Pick, K. Rolbiecki, and W. J. Stirling, *JHEP* **12** (2006) 007, [arXiv:hep-ph/0607104](https://arxiv.org/abs/hep-ph/0607104).
- [85] M. Bahr *et al.*, *Eur. Phys. J.* **C58** (2008) 639–707, [arXiv:0803.0883](https://arxiv.org/abs/0803.0883) [hep-ph].
- [86] S. Gieseke *et al.*, [arXiv:1102.1672](https://arxiv.org/abs/1102.1672) [hep-ph].
- [87] M. Gigg and P. Richardson, *Eur. Phys. J.* **C51** (2007) 989–1008, [arXiv:hep-ph/0703199](https://arxiv.org/abs/hep-ph/0703199).
- [88] H.-U. Martyn, [arXiv:hep-ph/0302024](https://arxiv.org/abs/hep-ph/0302024).
- [89] E. Boos, G. A. Moortgat-Pick, H. Martyn, M. Sachwitz, and A. Vologdin, [arXiv:hep-ph/0211040](https://arxiv.org/abs/hep-ph/0211040) [hep-ph].

- [90] E. Boos, H. Martyn, G. A. Moortgat-Pick, M. Sachwitz, A. Sherstnev, *et al.*, *Eur.Phys.J.* **C30** (2003) 395–407, [arXiv:hep-ph/0303110](#) [hep-ph].
- [91] M. M. Nojiri, K. Fujii, and T. Tsukamoto, *Phys.Rev.* **D54** (1996) 6756–6776, [arXiv:hep-ph/9606370](#) [hep-ph].
- [92] F. James and M. Roos, *Comput. Phys. Commun.* **10** (1975) 343–367.
- [93] F. James, *CERN Program Library Long Writeup D506* (1994) .
- [94] W. Oller, H. Eberl, and W. Majerotto, *Phys. Lett.* **B590** (2004) 273–283, [arXiv:hep-ph/0402134](#).
- [95] T. Fritzsche and W. Hollik, *Nucl. Phys. Proc. Suppl.* **135** (2004) 102–106, [arXiv:hep-ph/0407095](#).
- [96] P. Bechtle, K. Desch, W. Porod, and P. Wienemann, *Eur. Phys. J.* **C46** (2006) 533–544, [arXiv:hep-ph/0511006](#).
- [97] R. Lafaye, T. Plehn, M. Rauch, and D. Zerwas, *Eur. Phys. J.* **C54** (2008) 617–644, [arXiv:0709.3985](#) [hep-ph].